Supporting Information

Controllably Doping Nitrogen into 1T/2H MoS_2 Heterostructure Nanosheets Toward the Enhanced Supercapacitive and Electrocatalytic Performance by Low-Power N_2 Plasma

Kai Le[†,#], *Xiang Zhang*[‡], *Qi Zhao*[†,§], *Yuzhen Liu*[//], *Peng Yi*[†,§], *Shusheng Xu*[*,†,#], *and Weimin Liu*[†]

[†] The State Key Laboratory of Solid Lubrication, Lanzhou Institute of Chemical Physics, Chinese Academy of Sciences, Lanzhou 730000, China

[‡] State Key Laboratory of Crystal Materials, Institute of Crystal Materials, Shandong University, Jinan 250100, China

[#]Qingdao Center of Resource Chemistry & New Materials, Qingdao, 266071, China

[§]College of Mechanical and Electronic Engineering, China University of Petroleum, Qingdao 266580, China

[//]Department of Mechanical Engineering, Yonsei University, Seoul 03722, Republic of Korea

[*]*Corresponding author (e-mail: ssxu@licp.cas.cn)*

Supercapacitor performance measurements

The electrochemical tests including cyclic voltammogram (CV), galvanostatic charge-discharge (GCD), electrochemical impedance spectra (EIS) and cycling stability were firstly studied on a CS electrochemistry workstation in three-electrode system consistent of as-made working electrode, Pt foil counter electrode, Ag/AgCl reference electrode and 0.5M H_2SO_4 aqueous electrolyte. The EIS spectra were measured in the frequency from 10 kHz to 0.01 kHz at an open circuit potential with an AC amplitude of 5 mV. The cycling test was carried out through GCD. Then, the electrochemical performances of as-assembled FSSC devices were also investigated using a CS electrochemistry workstation in two-electrode system including CV, GCD and cycling tests. Both the specific capacitances of single electrode and FSSC device can be determined from the GCD curves through formula:

$$C = \frac{I \times \Delta t}{m \times \Delta V} \tag{S1}$$

where Δt, I, and ΔV are the discharge time, the charge-discharge current, and the potential range excluding IR drop in charge-discharge curves and m represents the mass loading of the working electrode.

HER performance measurement

The HER performances were also measured in three-electrode system with the 0.5M H_2SO_4 aqueous degassed by N_2 gas as electrolyte. All the electrochemical measurements were conducted on a CS electrochemical workstation. The linear sweep voltammetry (LSV) curves were measured at the scan rates 5 mV s^{-1} and all the LSV curves were IR corrected. All the potentials were converted to the potentials *versus* the reversible hydrogen electrode (RHE) according to following equation:

$$E_{\mathrm{REH}} = E_{\mathrm{Ag/AgCl}} + 0.0591\mathrm{pH} + 0.197 \quad \text{(S2)}$$

The Tafel slope could be obtained using the Tafel equation as follows:

$$\eta = a + b\lg(j) \quad \text{(S3)}$$

where j is the current density and b is the Tafel slope. CV was conducted at various scan rates in the potential range of 0.1 V-0.2 V (*vs.* RHE) to calculate Cdl. CV for stability testing was performed at a scanning rate of 50 mV/s for 1,000 cycles from 0 to -0.35 V *vs.* RHE. The EIS was measured in the frequency in the frequency from 10 kHz to 0.01 Hz at an amplitude of 5 mV at the overpotential of 100 mV *vs.* RHE.

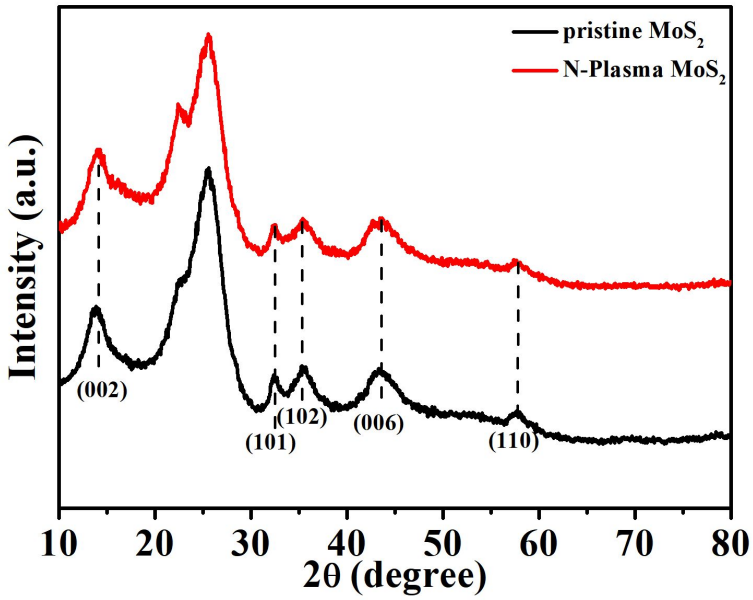

Figure S1. The XRD patterns of MoS_2 before and after N-plasma treatment.

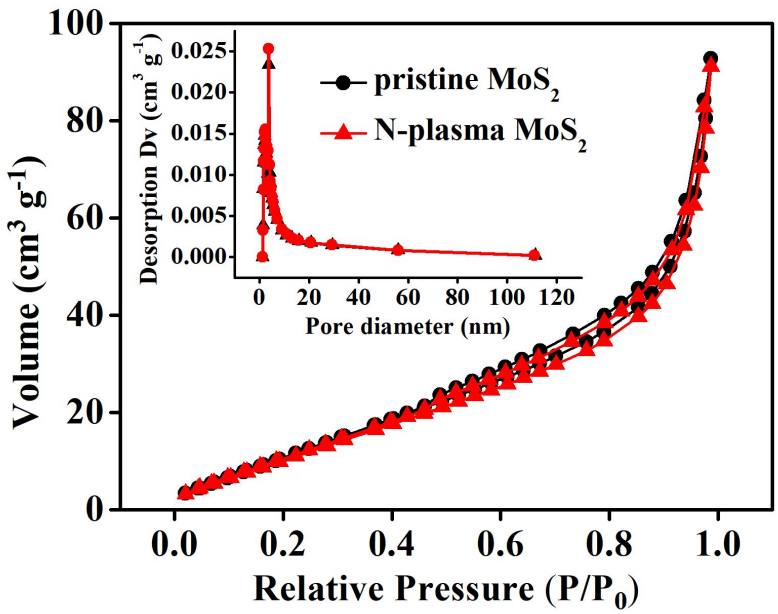

Figure S2. N_2 adsorption/desorption isotherms and pore size distribution (inset) of Pristine MoS_2 and N-plasma MoS_2.

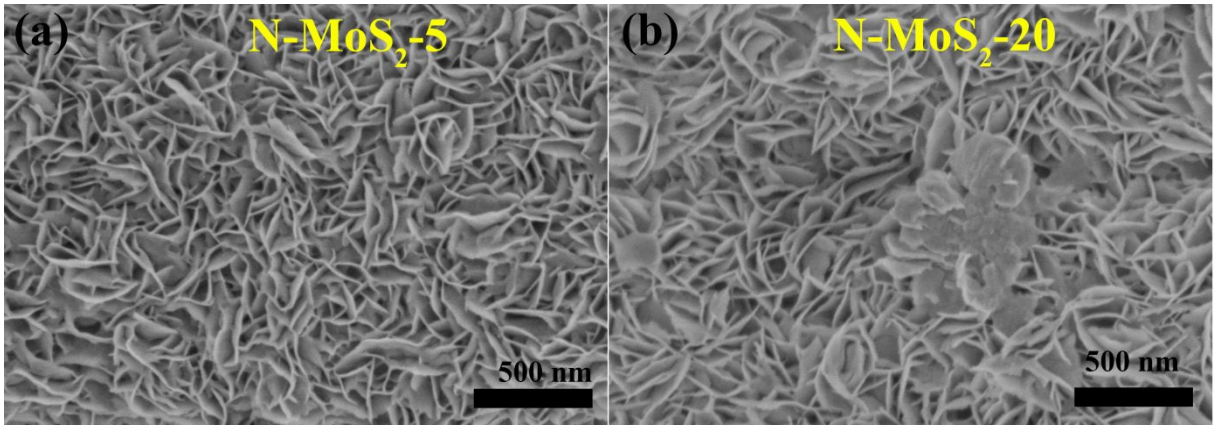

Figure S3. SEM images of (a) N-MoS_2-5 and (b) N-MoS_2-20.

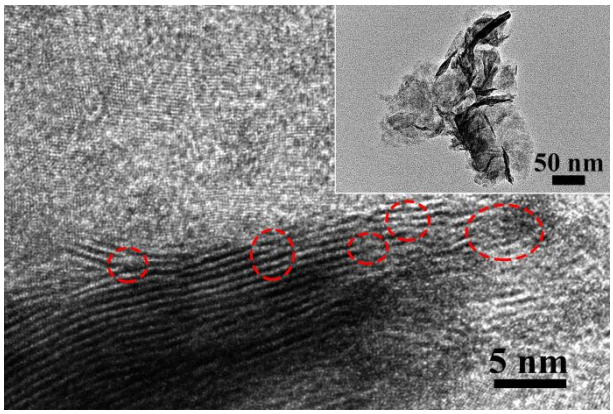

Figure S4. The TEM image of pristine MoS_2

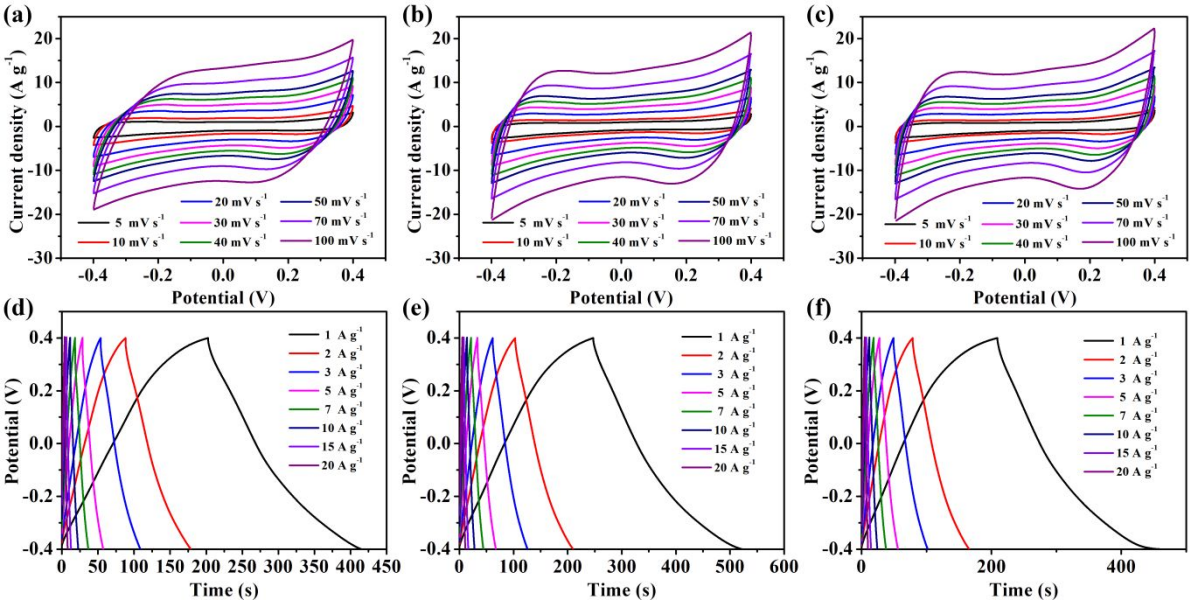

Figure S5. CV curves of (a) pristine MoS_2, (b) N-MoS_2-5 and (c) N-MoS_2-20 at different scan rates and GCD curves of (d) pristine MoS_2, (e) N-MoS_2-5 and (f) N-MoS_2-20 at various current densities.

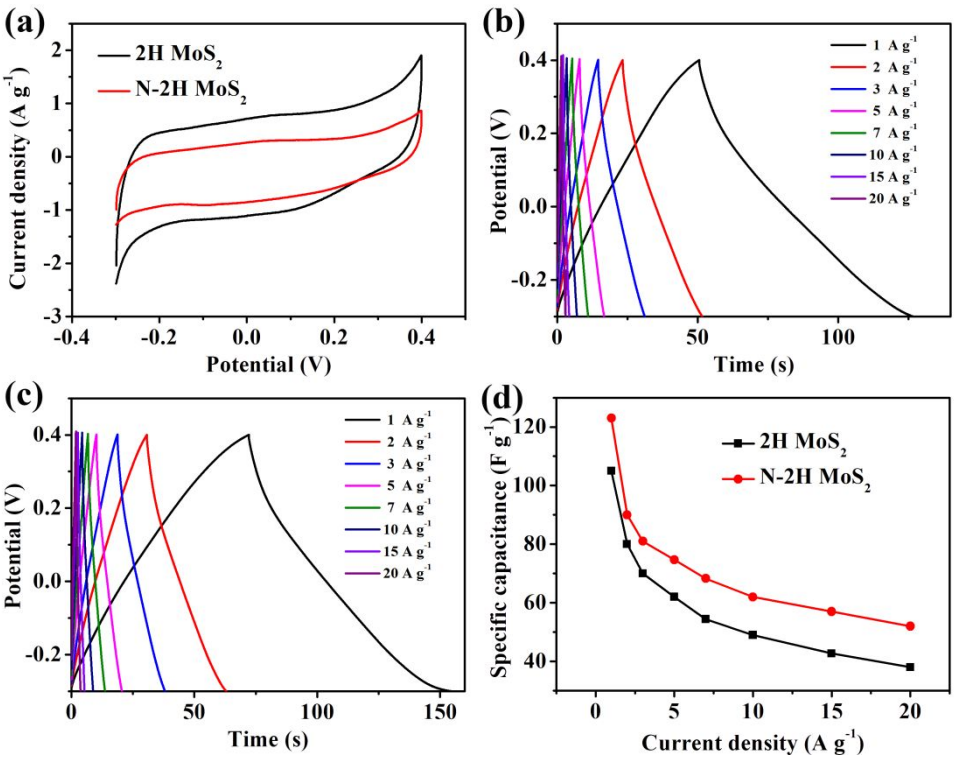

Figure S6. (a) CV curves of 2H MoS_2 and N-2H MoS_2 electrodes at 5 mV s^{-1}. GCD curves of (b) 2H MoS_2 and (c) N-2H MoS_2 electrodes. (d) Specific capacitance at different current densities of these electrodes.

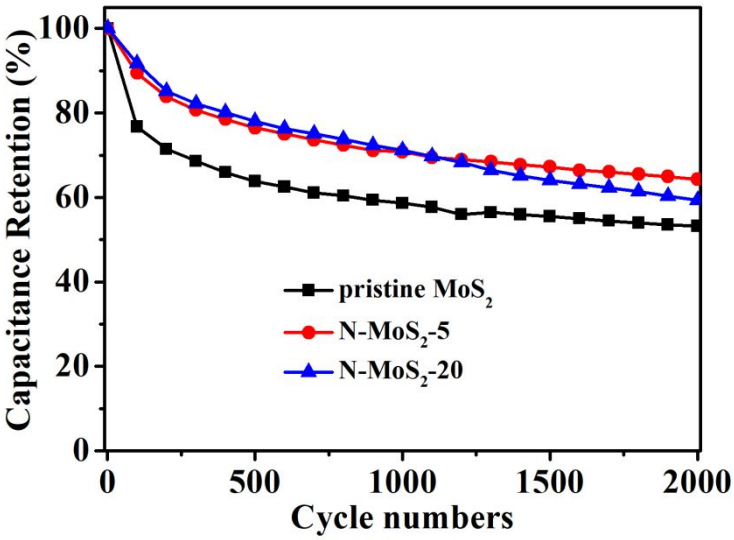

Figure S7. Cycling performance of pristine MoS_2, N-MoS_2-5 and N-MoS_2-20 electrodes.

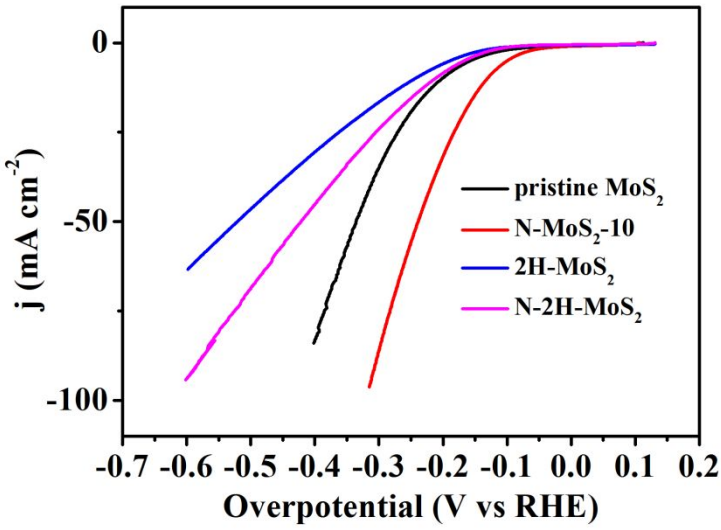

Figure S8. LSV curves of pristine MoS_2, N-MoS_2-10, 2H MoS_2 and N-2H MoS_2 in 0.5 M H_2SO_4 with a scan rate of 5 mV s^{-1}.

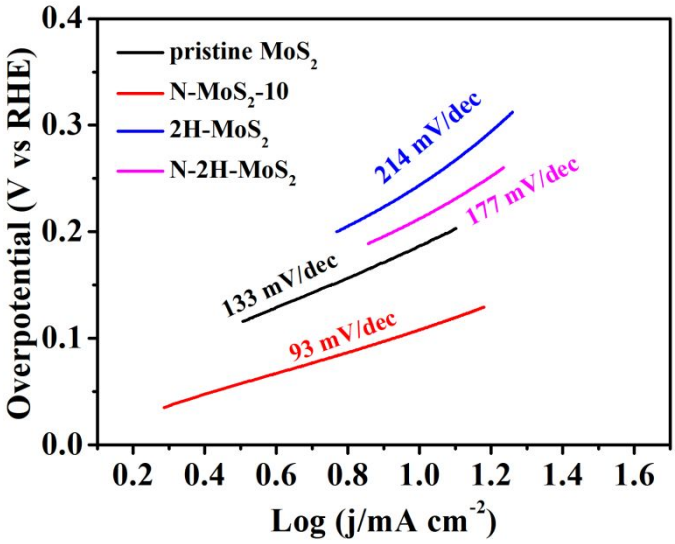

Figure S9. HER Tafel curves of pristine MoS_2, N-MoS_2-10, 2H MoS_2 and N-2H MoS_2.

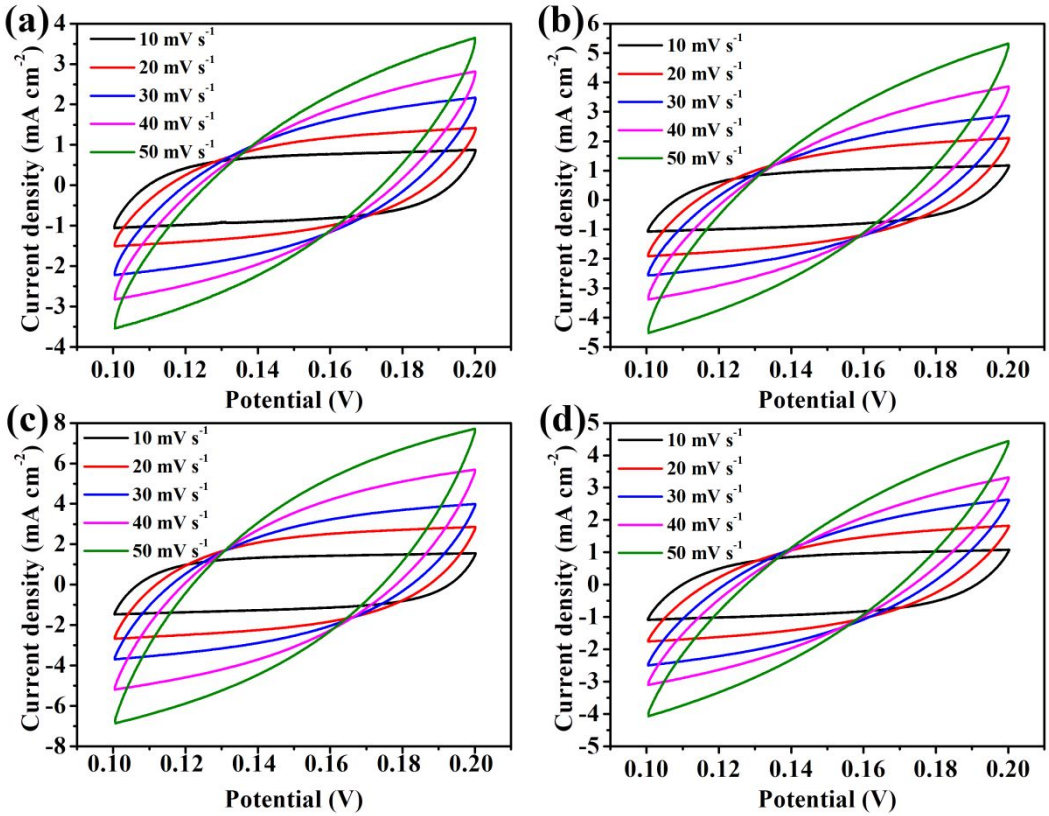

Figure S10. CV curves of (a) pristine MoS_2, (b) N-MoS_2-5, (c) N-MoS_2-10 and (d) N-MoS_2-20 at different scan rates in 0.5 M H_2SO_4.

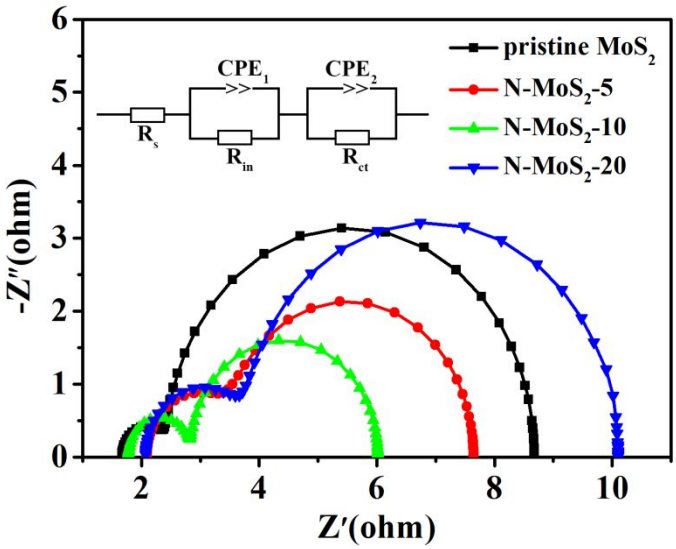

Figure S11. The EIS fitting results of the pristine MoS_2, N-MoS_2-5, N-MoS_2-10 and N-MoS_2-20.

Table S1. The normalized area ratio of the peaks of Mo $3p_{3/2}$ for Mo-N and pyridinic-N of these samples

Sample	**Mo $3p_{3/2}$**	**Mo-N**	**pyridinic-N**
pristine MoS_2	1	0.3	0.14
N-MoS_2-5	1	0.41	0.29
N-MoS_2-10	1	0.62	0.51
N-MoS_2-20	1	0.72	0.62

In order to precisely compare the content of nitrogen species of these samples, the peaks area values of them were normalized to the peak area of Mo $3p_{3/2}$.

Table S2. Comparison of HER activity for N-MoS2-10 with the recently-reported MoS_2 based HER catalysts under 0.5 M H_2SO_4.

Catalyst	Modulation strategy	Overpotential (10 mA cm^{-2})	Ref.
MoS_2 with S vacancies	hydrothermal growth and laser ablation in liquid	178 mV	1
Monolayer MoS_2 with S vacancies	NH_3 intercalation and ultrasonication	160 mV	2
Monolayer MoS_2 with S vacancies	CVD growth and remote H_2 plasma	183 mV	3
$MoSe_2/MoS_2$	Hydrothermal growth	162 mV	4
1T/2H MoS_2/carbon nanofiber	Hydrothermal growth	194 mV	5
N-MoS_2/3D carbon foam	Redox polymerization and sulfurization	155 mV	6
MoS_2 with single-atom vacancy	Hydrothermal growth and H_2O_2 chemical etching	131 mV	7
1T MoS_2	Hydrothermal growth	175 mV	8
Ni-Co-MoS_2	Precipitation and hydrothermal method	155 mV	9
Zn-doped MoS_2	Solvothermal growth and exfoliation	135 mV	10
1T/2H-MoS_2/graphene	Hydrothermal growth	143 mV	11
N-amorphous MoS_x	coprecipitation method	143 mV	12
N-doped 1T/2H MoS_2	Hydrothermal growth and low-power N_2 plasma at room temperature	131 mV	This work

RERERENCE

(1) Meng, C.; Lin, M.-C.; Du, X.-W.; Zhou, Y. Molybdenum Disulfide Modified by Laser Irradiation for Catalyzing Hydrogen Evolution. *ACS Sustain. Chem. Eng.* **2019,** *7* (7), 6999-7003.

(2) Xu, Y.; Wang, L.; Liu, X.; Zhang, S.; Liu, C.; Yan, D.; Zeng, Y.; Pei, Y.; Liu, Y.; Luo, S. Monolayer MoS_2 with S Vacancies from Interlayer Spacing Expanded Counterparts for Highly Efficient Electrochemical Hydrogen Production. *J. Mater. Chem. A* **2016,** *4* (42), 16524-16530.

(3) Cheng, C.-C.; Lu, A.-Y.; Tseng, C.-C.; Yang, X.; Hedhili, M. N.; Chen, M.-C.; Wei, K.-H.; Li, L.-J. Activating Basal-Plane Catalytic Activity of Two-Dimensional MoS_2 Monolayer with Remote Hydrogen Plasma. *Nano Energy* **2016,** *30*, 846-852.

(4) Li, S.; Zang, W.; Liu, X.; Pennycook, S. J.; Kou, Z.; Yang, C.; Guan, C.; Wang, J. Heterojunction Engineering of $MoSe_2/MoS_2$ with Electronic Modulation Towards Synergetic Hydrogen Evolution Reaction and Supercapacitance Performance. *Chem. Eng. J.* **2019,** *359*, 1419-1426.

(5) Niu, H.; Zou, Z.; Wang, Q.; Zhu, K.; Ye, K.; Wang, G.; Cao, D.; Yan, J. Structurally Stable Ultrathin 1T-2H MoS_2 Heterostructures Coaxially Aligned on Carbon Nanofibers Toward Superhigh-eEnergy-Density Supercapacitor and Enhanced Electrocatalysis. *Chem. Eng. J.* **2020,** *399*, 125672.

(6) Jia, X.; Ren, H.; Hu, H.; Song, Y. F. 3D Carbon Foam Supported Edge-Rich N-Doped MoS_2 Nanoflakes for Enhanced Electrocatalytic Hydrogen Evolution. *Chem. Eur. J.* **2020**, 26, 4150-4156.

(7) Wang, X.; Zhang, Y.; Si, H.; Zhang, Q.; Wu, J.; Gao, L.; Wei, X.; Sun, Y.; Liao, Q.; Zhang, Z.; Ammarah, K.; Gu, L.; Kang, Z.; Zhang, Y. Single-Atom Vacancy Defect to Trigger High-Efficiency Hydrogen Evolution of MoS_2. *J. Am. Chem. Soc.* **2020,** *142* (9), 4298-4308.

(8) Geng, X.; Sun, W.; Wu, W.; Chen, B.; Al-Hilo, A.; Benamara, M.; Zhu, H.; Watanabe, F.; Cui, J.; Chen, T.-p. Pure and Stable Metallic Phase Molybdenum Disulfide Nanosheets for Hydrogen Evolution Reaction. *Nat. commun.* **2016,** *7*.

(9) Yu, X.-Y.; Feng, Y.; Jeon, Y.; Guan, B.; Lou, X. W.; Paik, U. Formation of Ni-Co-MoS_2 Nanoboxes with Enhanced Electrocatalytic Activity for Hydrogen Evolution. *Adv. Mater.* **2016,** *28*, 9006-9011.

(10) Shi, Y.; Zhou, Y.; Yang, D. R.; Xu, W. X.; Wang, C.; Wang, F. B.; Xu, J. J.; Xia, X. H.; Chen, H. Y. Energy Level Engineering of MoS_2 by Transition-Metal Doping for Accelerating Hydrogen Evolution Reaction. *J. Am. Chem. Soc.* **2017,** *139*, 15479-15485.

(11) Xiao, Y.; Tan, M.; Li, Z.; He, L.; Gao, B.; Chen, Y.; Zheng, Y.; Lin, B. Ethylenediamine-Assisted Phase Engineering of 1T/2H–MoS_2/Graphene for Efficient and Stable Electrocatalytic Hydrogen Evolution. *Int. J. Hydrog. Energy* **2021,** *46*, 11688-11700.

(12) Ding, R.; Wang, M.; Wang, X.; Wang, H.; Wang, L.; Mu, Y.; Lv, B. N-Doped Amorphous MoS_x for the Hydrogen Evolution Reaction. *Nanoscale* **2019,** *11*, 11217-11226.